# Handling Uncertainties in Ground Risk Buffer Computation for Risk Assessment and Preparation of UAV Operations

Sylvain Bertrand, Stéphanie Lala, Nicolas Raballand

# Handling Uncertainties in Ground Risk Buffer Computation for Risk Assessment and Preparation of UAV Operations

Sylvain Bertrand[1], Stéphanie Lala[1], Nicolas Raballand[1]

***Abstract*— This paper proposes a method for computation of ground impact distance of Unmanned Aerial Vehicles (UAVs), in presence of uncertainties. Descent to ground is described as a sequence of different phases. For each phase, a model is derived to compute the ground distance traveled by the UAV. Uncertainties on different parameters or conditions can be handled by the proposed approach as well as their propagation through the sequence of computation models. It enables to estimate distribution of ground impact distances and help in designing the width of Ground Risk Buffers for UAV operations. An example of risk assessment involving this process is also proposed in the paper based on indexes derived from the SORA guidelines.**

## I. INTRODUCTION

Operating Unmanned Aerial Vehicles for long range missions, such as linear infrastructure inspection [1] or goods delivery [2], implies flights beyond visual line of sight over areas where risks may be implied for third parties at ground. It is therefore mandatory to have good evaluation of these risks during mission preparation, to design safety margins accordingly.

More specifically, Ground Risk Buffers (GRBs) can be defined from either sides of the flight volume of interest for the mission to ensure that an uncontrolled descent of the UAV to the ground will not lead to impacts with people in populated areas. The width of the buffer should be design cautiously as its underestimation may lead to uncontrolled risks and its overestimation may impose too restrictive constraints on the mission.

In Europe, risk assessment for medium size/mass vehicles involved in long range missions beyond line of sight has to be carried out by following the SORA guidelines from EASA [3]. One step of the SORA consists in evaluating the initial Ground Risk Class (iGRC) over the surface at ground covered by the flight volume including these GRBs. From this step and the following ones, Specific Assurance and Integrity Levels (SAIL) and Operational Safety Objectives (OSO) are derived. A good evaluation of the Ground Risk Class and therein an accurate design of the Ground Risk Buffers are of paramount importance.

Different methods have been proposed in the literature that can be used to estimate the ground impact distance of an UAV and help in the design of the GRBs. The work in [4] considered using a 6-dof dynamical model of aircraft to generate geometric ground impact footprints. Maximum ground impact distance can then be easily deduced from the footprint. In [5], a ballistic model including drag and effect of wind is considered to estimate the traveled distance at ground before impact and the impact probability distribution at ground accounting for uncertainties on some parameters. This model has been used in [6] to assess risk at ground for people. Generation of ground impact footprints and impact probability maps have also been investigated by the authors in [7], [8] and [9] by respectively proposing methods based on Monte Carlo simulations, neural networks or importance sampling. Ground impact distance corresponding to a certain level of confidence can be deduced from these models. It is worth mentioning that some of these works, such as [5], can be applied to fixed-wing or multi-rotor UAVs, although other considering more detailed dynamics are specific to a given type of vehicle (eg. [10], or [11] for the descent trajectory of a quadrotor UAV in case of propeller failure).

In most of the aforementioned works, the descent trajectory under study is usually composed of a single phase governed by the same motion model. In practice, several different phases must be considered between the instant of loss of control of an UAV and its impact to the ground. These can be for example: acceleration of the platform (eg. during a fly-away phase), activation of a Flight Termination System (FTS) (eg. motors turn off), deployment of a safety parachute, final descent to ground, etc. During all these phases, distance traveled at ground by the UAV should be computed and accounted for in the determination of the total ground distance between time of failure and ground impact. This total ground impact distance is of importance for the determination of GRBs that will ensure a safety margin between the operational volume of flight and third-parties at ground.

In this paper, a method is proposed for computation of the ground impact distance of UAVs by decomposing its descent into several phases to which traveled distance computation models are associated. Once identified for each of the models, uncertainties on initial conditions and/or parameters can be taken into account and propagated through the sequence of computation models. Ground impact distance and its distribution can hence be computed, which is of interest for GRB design. Analyzing the effect of each source of uncertainty, as proposed in this paper, also enables to identify the most impacting parameters, the effect of the knowledge on their level of uncertainty, and the contributions of the different phases of the descent to the value and dispersion of the ground impact distance.

The paper is organized as follows. The next two sections

[1]All authors are with Université Paris-Saclay, ONERA, Traitement de l'Information et Systèmes, 91123, Palaiseau, France {sylvain.bertrand, stephanie.lala, nicolas.raballand}@onera.fr

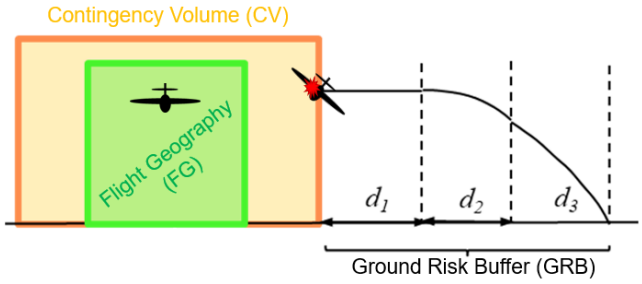


Fig. 1. Definition of the risk model introduced by SORA

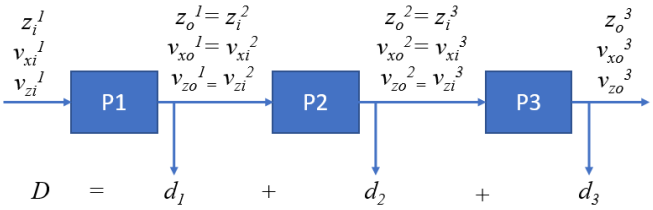


Fig. 2. Linking distance computation models in case of a descent to ground composed of three phases P1, P2, P3

present the context and main steps of the proposed approach. After introducing some notations and parameterizations in Section IV, Sections V and VI are devoted to the description of the different ground descent phases and their models, and computation of the ground impact distances. Section VII and VIII focus on uncertainties handling in the ground distance computations to define GRB width. Before concluding remarks, Section IX proposes an illustration example of risk assessment of an UAV mission using the GRB previously defined.

## II. CONTEXT

The context of this study is the one of long range operations, such as inspection of linear infrastructures. The type of drone under consideration is an UAV of medium size and mass that would be operated Beyond Visual Line of Sight (BVLOS) and hence fall within the *Specific* category as defined in E.U. regulations by the European Union Aviation Safety Agency (EASA). In that case, Predefined Risk Assessment should be carried out, eg. following the SORA guidelines.

In the SORA guidelines, evaluation of ground risk is based on the decomposition of the Operational Volume (OV) for the flight into two different parts (see Figure 1) which are:

- the *Flight Geography* (FG) devoted to the nominal part of the flight,
- the *Contingency Volume* (CV) inside which procedures must be triggered to make the drone fly back to the FG.

In case of failure in maintaining the drone inside the OV, a Flight Termination System (FTS) must be activated when the drone is exiting the CV. To account for this flight termination, a Ground Risk Buffer (GRB) is therefore defined on each side of the OV, corresponding to lateral safety margins that must be observed with respect to third parties at ground. Computation of the GRB width is of paramount importance, since its underestimation may lead to unconsidered risks for third-parties. On the contrary, overestimating the GRB width in a too conservative way may reduce the OV and restrict operational uses.

## III. MAIN STEPS OF THE APPROACH

The proposed approach is divided into three main steps which are:

- Step 1: Identification of the different phases of the descent to ground
- Step 2: Description of each phase
- Step 3: Identification of sources of uncertainties in the descriptions of the phases

**Step 1** consists in identifying the different phases the sequence of which characterizes the motion of the drone from its exit instant from the CV to the instant of ground impact.

In **Step 2**, a description of each of this phases should be performed. The objective is to describe the model and its underlying assumptions that can be used to compute the lateral distance traveled by the drone during the phase. Parameters used in the model are listed. As one is interested in computing the lateral distance wrt the CV, the model should describe the motion of the UAV in the $(x, z)$-plane (see reference frames in Figure 3). The inputs (denoted with index $i$) of the model associated to phase $k$ are the altitude $z_i^k$, and the velocity components $v_{xi}^k, v_{zi}^k$ of the drone. The outputs (denoted with index $o$) computed by the model related to phase $k$ are the altitude $z_o^k$ and the drone velocity components $v_{xo}^k, v_{zo}^k$ at the end of the phase, as well as the ground distance $d^k$ traveled by the drone during phase $k$.

Finally, **Step 3** consists in identifying the sources of uncertainties in the distance computation models associated to each phase. Different sources of uncertainties can be considered, for example:

- uncertainties on the inputs of the computation chain, eg. on the initial altitude $z_i^1$ at which the drone is exiting the CV, or on parameters defining velocity components $v_{xi}^1, v_{zi}^1$.
- uncertainties on some parameters used in the computation models, eg. time duration of a phase, aerodynamic coefficient, etc.

In the case of multiple phases, the models can be linked, using $(z_i^k, v_{xi}^k, v_{zi}^k) = (z_o^{k-1}, v_{xo}^{k-1}, v_{zo}^{k-1})$, to compute distance $d^k$ associated to each phase $k$, and finally the total ground impact distance $D = \sum_k d^k$ that can be used to defined the GRB (see example in Figure 2 with a ground descent decomposed into three phases).

To deal with uncertainties in the computation of the distances, different methods can be used. A worst case approach can be chosen by considering conservative bounds on some of the parameters. Methods such as interval analysis can be used to compute and propagate bounds to each intermediate variables of the computations and resulting distances.

Another possibility is to assume stochastic distributions for uncertain parameters. Monte Carlo simulations can be used to deal and propagate uncertainties in the computations of

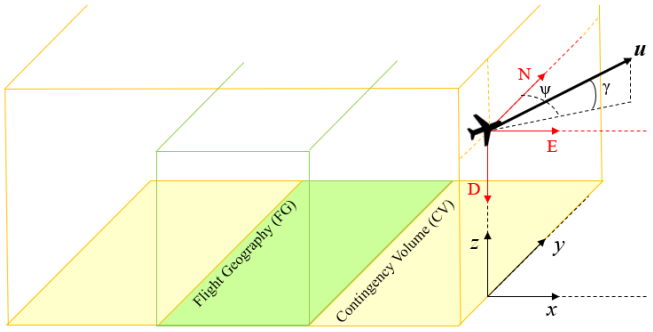


Fig. 3. Reference frames and notations associated to the UAV at the moment of exiting the CV

the distances and estimate their distributions. This is the approach that has been chosen in this paper.

As application example, it is assumed in the rest of the paper that the drone under consideration is a fixed-wing UAV equipped with an emergency parachute that is automatically triggered when the drone exits the CV.

The next section introduces some notations and parameterization that will be used in the descriptions of the models.

## IV. Reference frames and parameterization

### A. Reference frames

To describe the motion of the UAV during its descent to ground, following exit from the CV, two reference frames are defined (see Figure 3). The first one is a $(N, E, D)$ reference frame, with origin attached to the UAV at the instant of exit from the CV. Without loss of generality, it is assumed that the $N$ direction is aligned with the local boundary of the CV at this point and $E$ is normal to it. The second frame is the $(x, y, z)$ frame with origin at the ground projection of the UAV position at the instant of exit from the CV. This frame will be used to describe the descent motion to the ground. More specifically, as one is interested in the lateral distance computation wrt the CV, the descent motion of the drone will be studied in the $(x, z)$ plane, and distances traveled by the drone during each phase along the $x$-axis will be computed.

### B. Parameterization

It is assumed that the direction of exit of the CV by the drone is defined by the vector

$$\mathbf{u} = \begin{bmatrix} \sin(\psi)\cos(\gamma) \\ \cos(\psi)\cos(\gamma) \\ -sin(\gamma) \end{bmatrix} \quad (1)$$

where $\psi$ is the heading angle wrt the CV boundary, and $\gamma$ the flight path angle wrt the local horizontal (cf. Figure 3).

In the same way, the direction of the wind is defined using the angles $\psi_w$ and $\gamma_w$ and the vector

$$\mathbf{u_w} = \begin{bmatrix} \sin(\psi_w)\cos(\gamma_w) \\ \cos(\psi_w)\cos(\gamma_w) \\ -sin(\gamma_w) \end{bmatrix} \quad (2)$$

The wind velocity vector wrt ground is then $\mathbf{v_w} = V_w \mathbf{u_w}$ where $V_w$ is the speed magnitude.

In a conservative way, it is assumed that the velocity vector of the drone $\mathbf{v_i^1}$ considered as initial condition to the (first phase of the) ground descent is composed of the nominal speed $V_{nom}$ of the drone for its mission, oriented towards the exit direction, augmented by the wind velocity, that is:

$$\mathbf{v_i^1} = \begin{bmatrix} v_{xi}^1 \\ v_{yi}^1 \\ v_{zi}^1 \end{bmatrix} = V_{nom}\mathbf{u} + \mathbf{v_w} = V_{nom}\mathbf{u} + V_w\mathbf{u_w} \quad (3)$$

## V. Identification and description of the phases

### A. Phases identification

For the illustration case under consideration in this paper, it is assumed that the descent to the ground can be decomposed into a sequence of three phases, as illustrated on Figures 1 and 2, which are:

- Phase no1 (P1): detection of exit from CV by the drone and activation of the FTS.
- Phase no2 (P2): Deployment of the safety parachute
- Phase no3 (P3): Descent to ground under parachute

### B. Description of Phase 1 - CV exit detection and FTS activation

In this first phase (P1), it is assumed that the drone is equipped with a system that is able to detect the exit from the CV and automatically trigger a FTS that will turn the engine off and eject an emergency parachute. The time duration related to this process is denoted by $T_{FTS}$.

To be conservative as much as possible for the ground distance computation, it is assumed that the engine thrust of the drone is at its maximum during this phase, before being turned off by the FTS, leading to an acceleration vector $A_{max}\mathbf{u}$ of magnitude $A_{max}$.

Therefore, the following equations are considered to compute distance $d_1$ and output variables $(z_o^1, v_{xo}^1, v_{zo}^1)$ of this first phase:

$$d_1 = \frac{1}{2}A_x T_{FTS}^2 + v_{xi}^1 T_{FTS} \quad (4)$$

$$z_o^1 = \frac{1}{2}(A_z - g)T_{FTS}^2 + v_{zi}^1 T_{FTS} + z_i^1 \quad (5)$$

$$v_{xo}^1 = A_x T_{FTS} + v_{xi}^1 \quad (6)$$

$$v_{zo}^1 = (A_z - g)T_{FTS} + v_{zi}^1 \quad (7)$$

with $A_x = A_{max}\sin(\psi)\cos(\gamma)$ and $A_z = -A_{max}\sin(\gamma)$ the components of the acceleration vector, assumed to be constant during Phase 1, and $z_i^1$ the altitude of the drone at the exit instant from the CV.

### C. Description of Phase 2 - Safety parachute deployment

Let denote by $t_i^2$ the initial instant of Phase 2 (P2), which corresponds to the final one of Phase 1, and is the instant of ejection of the parachute.

In P2, it is assumed that the efficiency of the parachute is increasing from that ejection instant $t_i^2$ to the instant of

its full deployment, denoted $t_o^2$. The deployment duration, which therefore characterizes this phase, is assumed to be given and denoted by $T_{dep}$, and one has $t_o^2 = t_i^2 + T_{dep}$.

During P2, the dynamics of the drone in the $(x, y, z)$ frame are assumed to be described by:

$$\dot{\mathbf{p}} = \mathbf{v}, \qquad \dot{\mathbf{v}} = \mathbf{g} + \frac{\mathbf{1}}{\mathbf{m}}\mathbf{F_a} \tag{8}$$

with the position vector $\mathbf{p}$ of the drone, the gravity vector $\mathbf{g}$, the mass $m$ and the aerodynamic force $\mathbf{F_a}$ due to the effect of the parachute. In a first approximation, assuming that the parachute and the drone are aligned along the motion direction, this force can be described by

$$\mathbf{F_a} = -mK \left\|\mathbf{v} - \mathbf{v_w}\right\| (\mathbf{v} - \mathbf{v_w}) \tag{9}$$

with $\mathbf{v}$ and $\mathbf{v_w}$ being respectively the drone and wind velocity vectors wrt ground. The coefficient $K$ is defined by $K = \frac{1}{2}\rho\frac{SC_D}{m}$, where $\rho$ is the air density, $S$ is the apparent surface, $C_D$ the aerodynamic coefficient and $m$ the mass of the system "drone + parachute".

During phase P2, it is assumed that $K$ is linearly increasing during the deployment duration $T_{dep}$ as

$$K(t) = K_{max}\frac{t - t_i^2}{T_{dep}}, \forall t \in \left[t_i^2, t_i^2 + T_{dep}\right] \tag{10}$$

where $K_{max}$ is the maximum value of $K$ when the parachute is fully deployed and is at its maximum efficiency. The value $K_{max}$ can be deduced from the resulting vertical speed under parachute fully deployed $v_z^{par}$ at equilibrium descent given by

$$K_{max} = \frac{g}{(v_z^{par})^2} \tag{11}$$

To compute ground distance $d_2$ along the $x-$axis and output variables $(z_o^2, v_{xo}^2, v_{zo}^2)$ associated to phase P2, equations (8)-(9)-(10) are integrated over the time duration $T_{dep}$ from the initial condition $(z_i^2, v_{xi}^2, v_{zi}^2) = (z_o^1, v_{xo}^1, v_{zo}^1)$.

### *D. Description of Phase 3 - Descent to ground under parachute*

The third and last phase of the descent (P3) corresponds to a descent under parachute fully deployed. The dynamics of the system "drone + parachute" is assumed to be described by the same equations as for phase P2, i.e. (8)-(9), but with $K = cste = K_{max}$. These equations are integrated from the initial condition $(z_i^3, v_{xi}^3, v_{zi}^3) = (z_o^2, v_{xo}^2, v_{zo}^2)$ until the altitude $z$ of the drone becomes zero (ground impact) ($z_o^3$ =0). Then the distance $d_3$ can be deduced as well as impact velocity components $(v_{xo}^3, v_{zo}^3)$.

## VI. Ground impact distance computation

Models described in the previous section can be linked together to simulate the sequence of phases representing the ground descent. Examples of descent trajectories corresponding to the sequence of P2 and P3 are presented in Figure 4. The initial condition in $x$ is chosen to be equal to zero and parameters used for this computation are given in Table I.

| Parameter | Value | Unit | Parameter | Value | Unit |
|---|---|---|---|---|---|
| $m$ | 15 | kg | $V_{nom}$ | 13.9 | m/s |
| $A_{max}$ | 2.8 | m/s$^2$ | $S$ | 4 | m$^2$ |
| $\rho$ | 1.225 | kg/m$^3$ | $g$ | 9.81 | m/s$^2$ |
| $z_i^1$ | 100 | m | $\gamma$ | 0 | deg |
| $T_{FTS}$ | 0.4 | s | $T_{dep}$ | 2 | s |
| $v_z^{par}$ | -0.5 | m/s | | | |

TABLE I
Summary of parameters' values

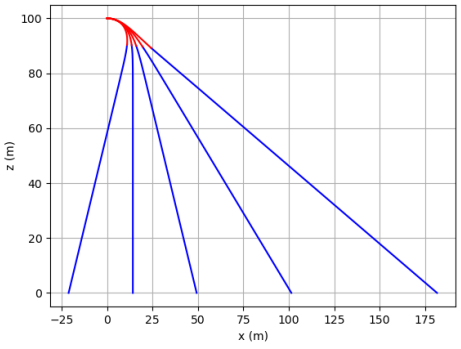


Fig. 4. Examples of descent trajectories during phases P2 (red) and P3 (blue) for different values of wind: from left to right -2, 0, 2, 5, 9.7 m/s

The red part of the trajectories correspond to P2 whereas the blue one corresponds to P3.

Using the models of the three phases according to the scheme presented in Figure 2 enables to compute the distances $d_1, d_2, d_3$ and the ground impact distance $D$.

It is assumed that the wind remains horizontal, i.e. $\gamma_w = 0$, and constant during the three phases. In a worst-case approach one considers that the wind velocity is directed along the $x$-axis, that is $\psi_w = \pi/2$. Distances $d_1, d_2, d_3$ of each phase and ground impact distance $D$ are presented in Figure 5 for different values of the wind magnitude, $V_w \in \{0, 2, 4, 6, 8, 10, 12\}$ m/s. Influence of wind on the ground impact distance is clearly visible. As can also be noticed, phase P3 provides the highest contribution to the ground impact distance $D$ in case of wind. If there is no wind, distance $d_3$ is close to zero as the ground descent under the fully deployed parachute is vertical (see also Figure 4).

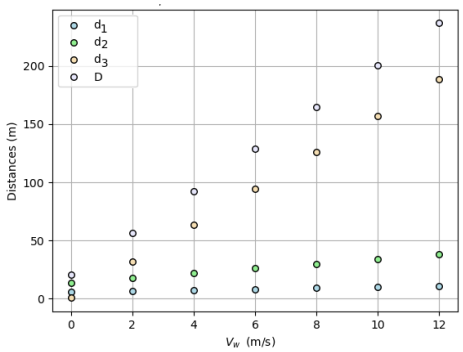


Fig. 5. Distances $d_1, d_2, d_3$ of each phase and ground impact distance $D$ for different values of wind $V_w$

## VII. Uncertainties

Different parameters are used in the representation of the CV's exit condition introduced in Section IV as well as the models described in Section V. In practice, it may be difficult to have a good knowledge of some of these parameters. Therefore, Step 3 of the proposed approach consists in identifying uncertainties.

Sources of uncertainties considered here, for this illustration case, are listed below along with chosen assumptions. They concern the exit conditions of the drone from the CV (altitude and velocity direction), the wind conditions, the duration of FTS activation and parachute deployment and the aerodynamic coefficient of the system "drone + parachute". Note that other sources of uncertainties could have been considered to extend further the analysis provided in this paper to illustrate the proposed approach (eg. horizontal localization accuracy of the drone, maximal acceleration during P1, etc.).

### A. Wind velocity

Aerological conditions may strongly vary during the flight and it is therefore not possible to accurately predict the wind encountered by the drone at the exit instant from the CV and during its ground descent. A conservative approach is hence adopted, by considering as worst case wrt the distance traveled during ground descent that the wind velocity is directed along the $x$-axis, i.e. $\psi_w = \pi/2$. It is furthermore assumed that wind is horizontal, i.e. $\gamma_w = 0$ and constant during the ground descent. In that case, the velocity vector for the wind is given by $\mathbf{v_w} = [V_w \quad 0 \quad 0]^\top$ in the $(x, y, z)$ frame. For conservatism, the wind magnitude $V_w$ will be chosen as the maximum value that the drone is able to manage in flight (drone characteristics). It is assumed that in case of aerological conditions with greater wind speed, the mission would not have been started.

The value $V_w = 9.7$m/s has been chosen for the rest of the paper. Using this value along with parameters given in Table I results in a ground impact distance $D$ =195m.

### B. Altitude of the drone when exiting CV

As a worst case scenario, the maximum possible altitude of the drone should be considered. This maximum value can be chosen as the upper bound on the altitude defining the CV outer boundary. Nevertheless, due to non perfect accuracy of the drone localization system, the altitude at which the FTS will be activated may suffer from some uncertainties. Uncertainties will therefore be considered for the initial altitude $z_i^1$ of the drone at the exit instant from the CV. A normal distribution $z_i^1 \sim \mathcal{N}(\mu_{z_i^1}, \sigma^2_{z_i^1})$ has been chosen with mean $\mu_{z_i^1} = 100$m and standard deviation $\sigma_{z_i^1}$. Figure 6 presents distributions of the ground impact distance $D$ obtained by Monte Carlo simulations, considering $V_w = 9.7$ m/s and other parameters as in Table I. Results are presented for different values of $\sigma_{z_i^1}$ to emphasize its influence. This can be of particular interest in case the level of uncertainty cannot be accurately known or quantified. For each distribution of $D$, mean (red point), median (black point), percentiles (dashed and plain lines) and values at +/- 3 standard deviations (red crosses) are presented.

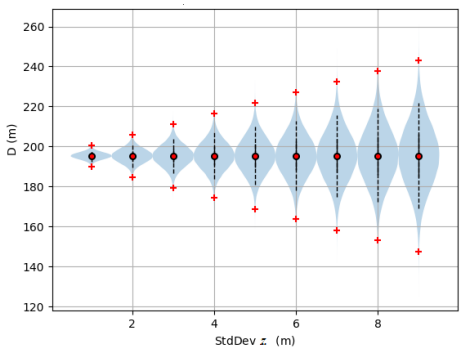


Fig. 6. Distributions of ground impact distance $D$ wrt standard deviation $\sigma_{z_i^1}$ on the initial altitude $z_i^1$.

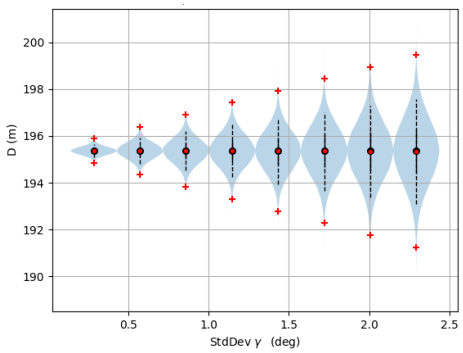


Fig. 7. Distributions of ground impact distance $D$ wrt standard deviation $\sigma_\gamma$ on the angle $\gamma$.

Let consider $\sigma_{z_i^1} = 2$m as the level of uncertainty corresponding to the localization system of the drone. According to Figure 6, this uncertainty would result in an additional margin[1] of 6m above the mean value of 195m for the ground impact distance $D$.

### C. Velocity direction of the drone when exiting CV

When leaving the FG and entering the CV, specific procedures must be triggered to make the drone re-entering the FG. In case of failure of such procedures, the way the drone will cross and exit the CV may not be fully predictable. For conservatism, it is assumed in this paper that $\psi = \pi/2$, i.e. a worst-case direction normal to the CV boundary. As horizontal flight may not be guaranteed, uncertainty on $\gamma$ will nevertheless be considered.

A normal distribution $\gamma \sim \mathcal{N}(\mu_\gamma, \sigma^2_\gamma)$ has been chosen with mean $\mu_\gamma = 0$ deg and standard deviation $\sigma_\gamma$. Figure 7 presents distributions of the ground impact distance $D$ obtained by Monte Carlo simulations, considering $V_w = 9.7$ m/s and other parameters as in Table I, for different values of $\sigma_\gamma$ to emphasize its influence. Let consider $\sigma_\gamma = 1.4$ deg as the level of uncertainty corresponding to exit condition of the drone. According to Figure 7, this uncertainty

[1] considering the value corresponding to the 95% percentile

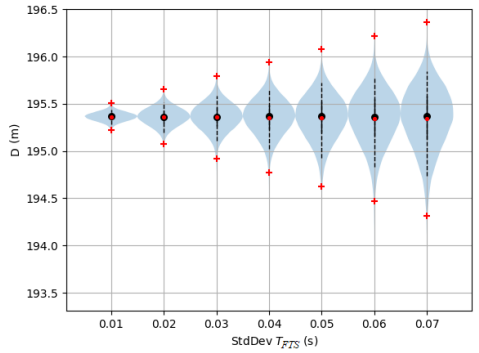


Fig. 8. Distributions of ground impact distance $D$ wrt standard deviation $\sigma_{T_{FTS}}$ on the duration $T_{FTS}$.

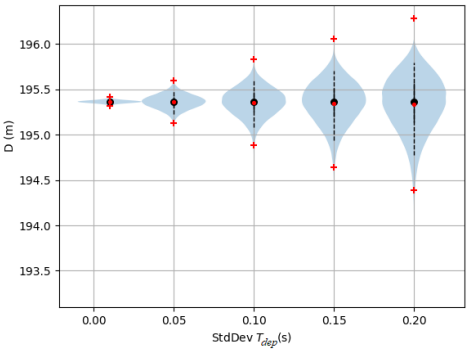


Fig. 9. Distributions of ground impact distance $D$ wrt standard deviation $\sigma_{T_{dep}}$ on the duration $T_{dep}$.

would results in an additional margin of 1.75m above the mean value of 195m for the ground impact distance $D$.

### D. Time durations of P1 and P2

For phase P1, it can be considered that $T_{FTS}$ representing the time duration of detection from CV and trigger of the FTS (engine shut down + ejection of safety parachute) during phase P1 may be subject to some variations. Uncertainties will be considered at a small level in this paper since it is assumed that an automatic system is in charge of this process. Note that in the case of a process involving an emergency alarm and a decision by a human operator, the corresponding uncertainty level can be much more important.
A normal distribution $T_{FTS} \sim \mathcal{N}(\mu_{T_{FTS}}, \sigma^2_{T_{FTS}})$ has been chosen with mean $\mu_{T_{FTS}}$ =0.4s and standard deviation $\sigma_{T_{FTS}}$.

For phase P2, uncertainties will also be considered on the duration $T_{dep}$ of the safety parachute deployment. A normal distribution $T_{dep} \sim \mathcal{N}(\mu_{T_{dep}}, \sigma^2_{T_{dep}})$ (s) has been chosen with mean $\mu_{T_{dep}}$ =2s and standard deviation $\sigma_{T_{dep}}$.

Similarly to what has been shown before regarding other parameters, resulting distributions of $D$ for different values of $\sigma_{T_{FTS}}$ or $\sigma_{T_{dep}}$ are respectively presented on Figure 8 and Figure 9. As an example, considering $\sigma_{T_{FTS}} = 0.05$s or $\sigma_{T_{dep}} = 0.5$s as level of uncertainty would imply respectively an additional margin on $D$ respectively of 0.7m or 1m.

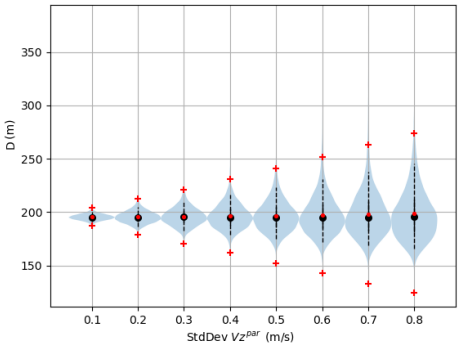


Fig. 10. Distributions of ground impact distance $D$ wrt standard deviation $\sigma_{v_z^{par}}$ on the vertical speed $v_z^{par}$ under parachute.

| Parameter | $z_i^1$ | $\gamma$ | $T_{FTS}$ | $T_{dep}$ | $v_z^{par}$ | All |
|---|---|---|---|---|---|---|
| Margin on D (m) | 6 | 1.75 | 0.7 | 1 | 28.4 | 55 |

TABLE II
MARGIN ON $D$ RELATED TO INDIVIDUAL EFFECT OF UNCERTAINTY ON EACH PARAMETER ($V_w = 9.7$ M/S)

### E. Aerodynamic coefficient

The aerodynamic coefficient $C_D$, or equivalently the coefficient $K$, involved in equation (9) is also subject to uncertainties. Its value can be deduced from the vertical speed $v_z^{par}$ under parachute fully deployed during equilibrium descent, as $C_D = mg/(2\rho S(v_z^{par})^2)$. Therefore uncertainty on the aerodynamic coefficient $C_D$ is handled by considering uncertainties on $v_z^{par}$ which is a quantity more easily obtained, eg. by return on experiments.
A normal distribution $v_z^{par} \sim \mathcal{N}(\mu_{v_z^{par}}, \sigma^2_{v_z^{par}})$ has been chosen with mean $\mu_{v_z^{par}}$ =-5.5 m/s and standard deviation $\sigma_{v_z^{par}}$. Figure 10 presents resulting distributions on $D$ wrt to different values of $\sigma_{v_z^{par}}$. A value of $\sigma_{v_z^{par}} = 0.5$m would lead to an additional margin of 28.4m on $D$.

### F. Analysis of the individual effect of each parameter uncertainty

The individual effect of uncertainty on each parameter has been analyzed on the resulting distributions of the ground impact distance $D$. From these distributions, some margin on $D$ can be determined. They are summarized in Table II. For the values considered for illustration purpose in this paper, it can be concluded that the most impacting parameters are $v_z^{par}$, or equivalently the aerodynamic coefficient, and the initial altitude $z_i^1$ . This type analysis is of interest to identify the most influencing parameter(s) and therefore to allow more effort on improving their identification, the design of some parts of the UAV or of its procedures involving these parameters, etc. This may influence the value of these parameters and/or the knowledge of their associated uncertainty, giving more accurate estimation of the ground impact distance $D$ and associated margin.

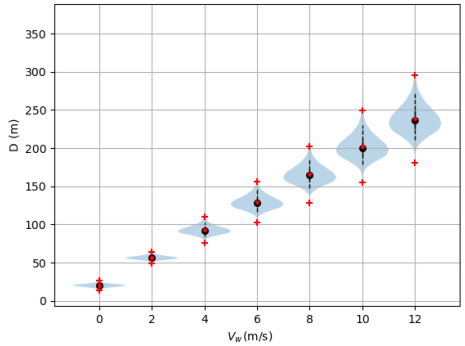


Fig. 11. Distributions of ground impact distance $D$ wrt values of wind speed $V_w$ (all uncertainties considered)

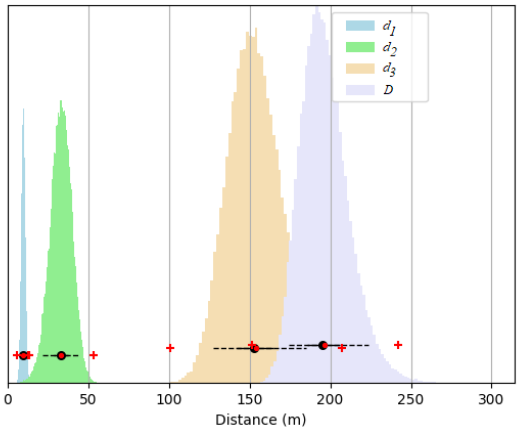


Fig. 12. Distributions of distances $d_1, d_2, d_3$ and ground impact distance $D$ (all uncertainties considered)

## VIII. Combined effect of uncertainties

In the previous section, individual effect of the uncertainty on each parameter has been analyzed separately. In this section, one is interested in analyzing the combined effect of all these uncertainties.

If the levels of uncertainties are quite accurately known, one can generate by Monte Carlo simulations the resulting distributions of the ground impact distance $D$. For illustration purposes, one assumes the following levels of uncertainties: $\sigma_{z_i^1}$ =2m, $\sigma_\gamma$ =1.4deg, $\sigma_{T_{FTS}}$ =0.05s, $\sigma_{T_{dep}}$ =0.5s, $\sigma_{v_z^{par}}$ =0.5m. Regarding wind speed $V_w$, different maximal values are considered as $V_w \in \{0, 2, 4, 6, 8, 10, 12\}$m/s. Figure 11 presents the resulting distributions on the ground impact distance $D$ wrt wind speed $V_w$. Considering a given value of maximal wind, one can analyze the contributions of the different phases of the ground distance. An example is given on Figure 12 for $V_w$ =9.7m/s. As can be seen, in this illustrative case, the major contribution in terms of both mean value and dispersion of impacts is phase P2. From the distribution of $D$ one can deduce some margin that should be taken into account to define the width of the GRB to be used to analyze ground risks and ensure safety of the UAV mission. Whereas a ground impact distance computation without considering uncertainties would lead to consider a GRB width of 195m, considering the combined effect of all uncertainties would make to choose a GRB width of 250m (from the 99.9% percentile in the distribution of $D$ in Figure 12), therefore some additional margin of 55m.

This definition of GRB width will be used in the next section in a illustration of risk assessment of an UAV mission.

## IX. Application to risk assessment

### A. Mission definition

For illustration purpose, a flight trajectory of 60km long in South of France is considered. The geography of the mission includes some inhabited areas with different levels of density ranging from zero to approximately 4500 people/km$^2$. A corridor of 100m width is defined as FG volume centered on the nominal flight trajectory planed for the drone. The CV englobing the FG is defined by considering a total width of 300m. Finally a GRB is defined on each side of the CV. As mentioned in the previous section, a width of 250m is considered for each buffer at each side of the CV, therefore accounting for effects of uncertainties. Another case with the GRB width of 195m will be considered as comparison basis (not accounting for uncertainties).

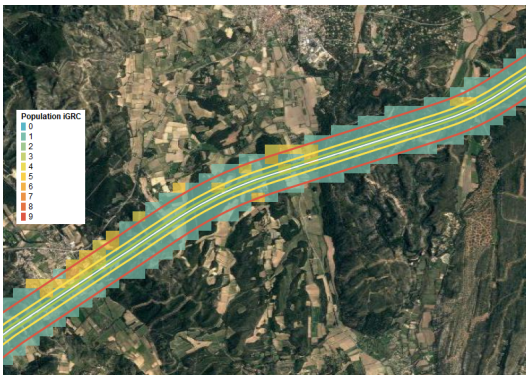


Fig. 13. Zoom on one part of the trajectory used for risk assessment

Figure 13 presents a zoom of the trajectory. The nominal flight trajectory planed for the drone is in white, the boundaries of the FG, CV and GRB in green, yellow and red respectively.

### B. Risk assessment

To evaluate the risks, the DROSERA tool [12] is used. It aims at quantifying the risks induced for third parties at ground likely to be overflown by a drone mission. To do this, it calculates an iGRC (intrinsic Ground Risk Class) index, as defined in the latest version of the SORA (2.5), and recalled here:

$$iGRC = \begin{cases} 1, \text{ if } \rho_{pop} = 0 \text{ or } \log_{10}(\rho_{pop} A_c) \leq -6 \\ \lceil 7 + \log_{10}(\rho_{pop} A_c) - 0.3 \rceil, \text{ else} \end{cases} \quad (12)$$

where $\rho_{pop}$ is the population density and $A_c$ = 16.1m$^2$ the Critical Area (cf. [3]) representing a collision surface between the drone and someone at ground.

Local values of this iGRC index are computed over the whole

possible impact footprint (FG+CV+GRBs) for the drone. They can be seen on Figure 13 as rectangles intersecting the footprint, which color represent the iGRC value. The size of the rectangles corresponds to the resolution of the population density data base.

Figure 14 presents the time evolution of the maximum value of local iGRC indexes computed in the instantaneous ground impact footprint of the drone. It helps to identify parts of the trajectory with highest iGRC values. Distribution of the local maximum iGRC is presented in Figure 15 which also constitutes another good indicator of the occurrence of the different risk levels over the mission. The iGRC value that will be considered for application of the SORA is the maximum value of these local iGRC indexes over the whole mission. For the illustrative example considered here, an iGRC of 6 would have been considered in the application of the SORA process.

All these indicators have been computed with a GRB width of 250m. Not considering effect of uncertainties, and hence using a GRB width of 195m, would have led to underestimate some risks, eg. some parts with densely populated area being possibly not considered (see example on Figure 16).

## X. CONCLUSIONS

In this paper, a method has been proposed to compute ground impact distance of a drone. The descent to ground is described as a sequence of different phases and a ground distance computation model is defined for each phase. It has been shown how to handle uncertainties and their propagation in the computations, to compute a distribution of the ground impact distance. Safety margin is then deduced to define the width of the Ground Risk Buffer used in mission preparation and risk assessment. An example of risk assessment has also been proposed based on risk index derived from the SORA guidelines.

Future work will address influence of other parameters in the computations, as well as applications to different types of UAVs and possible modes of failures leading to ground descents.

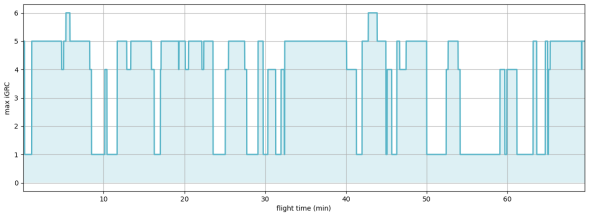


Fig. 14. Local maximum iGRC index wrt flight time

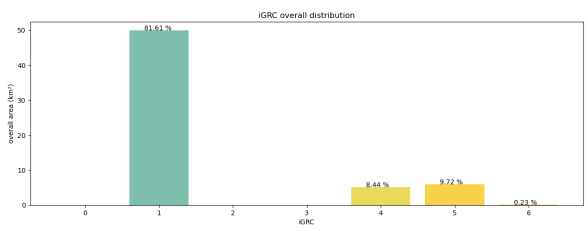


Fig. 15. Distribution of the local maximum iGRC index computed over the mission

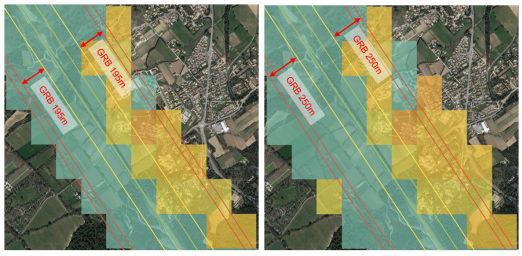


Fig. 16. iGRC index computed considering a GRB width of 195 m (left) or 250m (right)

## ACKNOWLEDGMENT

This work has been supported by French DGAC in the context of the research partnership PHYDIAS2 with ONERA for Safety Improvement of UAVs.

Developpement of the DROSERA tool has been supported by the research partnership between Altametris, RTE and ONERA on Risk Assessment of UAV Operations.

## REFERENCES

[1] S. Bertrand, N. Raballand, F. Viguier and F. Muller, "Ground risk assessment for long-range inspection missions of railways by UAVs", International Conference on Unmanned Aircraft Systems, Miami, FL, USA, 2017.

[2] P-C. Shao, "Risk Assessment for UAS Logistic Delivery under UAS Traffic Management Environment", in Aerospace, vol. 7, no. 10, 2020.

[3] EASA, "Easy Access Rules for Unmanned Aircraft Systems, Regulation (EU) 2019/947 and Regulation (EU) 2019/945", revision Sept. 2022.

[4] P. Wu, R. Clothier, "The development of ground impact models for the analysis of the risks associated with Unmanned Aircraft Operations over inhabited areas", 11th International Probabilistic Safety Assessment and Management Conference and the 2012 Annual European Safety and Reliability Conference, 2012.

[5] A. la Cour-Harbo, "Ground impact probability distribution for small unmanned aircraft in ballistic descent", International Conference on Unmanned Aircraft Systems, Athens, Greece, 2020.

[6] Y. Liu, X. Zhang, Z. Wang, Z. Gao, C. Liu, "Ground Risk Assessment of UAV Operations Based on Horizontal Distance Estimation under Uncertain Conditions", in Mathematical Problems in Engineering, 2021.

[7] B. Levasseur, S. Bertrand, N. Raballand, F. Viguier, G. Goussu, "Accurate Ground Impact Footprints and Probabilistic Maps for Risk Analysis of UAV Missions", IEEE Aerospace Conference, Big Sky, Montana, USA, 2019.

[8] B. Levasseur, S. Bertrand, N. Raballand, "Efficient Generation of Ground Impact Probability Maps by Neural Networks for Risk Analysis of UAV Missions", International Conference on Unmanned Aircraft Systems, Athens, Greece, 2020.

[9] J. Morio, B. Levasseur, S. Bertrand, "Drone Ground Impact Footprints with Importance Sampling: Estimation and Sensitivity Analysis", in Applied Sciences, vol. 11, no. 3871, 2021.

[10] Q. Jiao, Y. Liu, Z. Zheng, L. Sun, Y. Bai, Z. Zhang, L. Sun, G. Ren, G. Zhou, X. Chen, Y. Yan, "Ground Risk Assessment for Unmanned Aircraft Systems Based on Dynamic Model", in Drones, vol. 6, no. 11, 2022.

[11] M. H. Che Man, H. Hu, K. H. Low, "Crash Area Estimation for Ground Risk of Small Unmanned Aerial Vehicles Due to Propulsion System Failures", AIAA SciTech Forum, San Diego, CA, USA, 2022.

[12] N. Raballand, S. Bertrand, S. Lala, B. Levasseur, "DROSERA: a DROne Simulation Environment for Risk Assessment", 31st European Safety and Reliability Conference, Angers, France, 2021.